RAPID COMMUNICATION

High quality $PdTe_2$ thin films grown by molecular beam epitaxy*

RAPID COMMUNICATION

High quality $PdTe_2$ thin films grown by molecular beam epitaxy*

En Li(李恩)[1], Rui-Zi Zhang(张瑞梓)[1], Hang Li(李航)[1], Chen Liu(刘晨)[2], Geng Li(李更)[1], Jia-Ou Wang(王嘉鸥)[2], Tian Qian(钱天)[1], Hong Ding(丁洪)[1], Yu-Yang Zhang(张余洋)[1], Shi-Xuan Du(杜世萱)[1], Xiao Lin(林晓)[1,†], and Hong-Jun Gao(高鸿钧)[1,‡]

[1] *Institute of Physics & University of Chinese Academy of Sciences, Chinese Academy of Sciences, Beijing* 100190, *China*
[2] *Institute of High Energy Physics, Chinese Academy of Sciences, Beijing* 100049, *China*

(Received 28 April 2018; revised manuscript received 4 May 2018; published online 25 July 2018)

$PdTe_2$, a member of layered transition metal dichalcogenides (TMDs), has aroused significant research interest due to the coexistence of superconductivity and type-II Dirac fermions. It provides a promising platform to explore the interplay between superconducting quasiparticles and Dirac fermions. Moreover, $PdTe_2$ has also been used as a substrate for monolayer antimonene growth. Here in this paper, we report the epitaxial growth of high quality $PdTe_2$ films on bilayer graphene/SiC(0001) by molecular beam epitaxy (MBE). Atomically thin films are characterized by scanning tunneling microscopy (STM), X-ray photoemission spectroscopy (XPS), low-energy electron diffraction (LEED), and Raman spectroscopy. The band structure of 6-layer $PdTe_2$ film is measured by angle-resolved photoemission spectroscopy (ARPES). Moreover, our air exposure experiments show excellent chemical stability of epitaxial $PdTe_2$ film. High-quality $PdTe_2$ films provide opportunities to build antimonene/$PdTe_2$ heterostructure in ultrahigh vacuum for future applications in electronic and optoelectronic nanodevices.

Keywords: two-dimensional materials, transition-metal dichalcogenides, $PdTe_2$, molecular beam epitaxy

PACS: 68.37.Ef, 68.55.–a, 81.15.Hi, 61.05.jh **DOI:** 10.1088/1674-1056/27/8/086804

1. Introduction

Two-dimensional (2D) transition metal dichalcogenides (TMDs) have attracted extensive attention for applications in electronics,[1] optoelectronics[2,3] and valleytronics[4] due to their fantastic physical properties, including superconductivity,[5,6] charge density wave,[5,7] large non-saturating magnetoresistance,[8] sizable band gap,[9,10] and indirect-to-direct bandgap transition.[11] As one of the layered TMDs, $PdTe_2$ exhibits superconductivity below a transition temperature of about 1.7 K,[12,13] which is comparable to other TMD superconductors.[14] Moreover, Huang *et al.* predicted the existence of type-II Dirac fermions in $PtSe_2$ class,[15] including $PdTe_2$, as spin-degenerate counterparts of type-II Weyl fermions. Following Huang's predictions, the evidences of type-II Dirac cones in $PtSe_2$, $PtTe_2$, and $PdTe_2$ were soon characterized in angle-resolved photoemission spectroscopy (ARPES) experiments.[16–18] The coexistence of superconductivity and type-II Dirac cone in $PdTe_2$ makes it a possible platform to explore the interplay between superconducting quasi-particles and Dirac fermions.[18,19]

Furthermore, monolayer antimonene, a novel graphene-like 2D honeycomb lattice of antimony atoms with a bandgap of 2.28 eV,[20] has been grown on $PdTe_2$ substrates by molecular beam epitaxy (MBE).[21] Antimonene has been predicted for applications in photoelectric devices[22] due to the large bandgap and high-performance 2D field-effect transistors (FETs),[23] compliant with industry requirements for ultra-scaled channel length below 10 nm. High-quality single-crystalline $PdTe_2$ films will make it possible to build antimonene/$PdTe_2$ heterostructure for future applications in electronic and optoelectronic nanodevices. Therefore, the fabrication and study of high-quality $PdTe_2$ films are of high importance.

In this letter, we report the epitaxial growth of high-quality $PdTe_2$ films on bilayer graphene/SiC(0001) by MBE method. The stoichiometry and quality of the epitaxial film are verified by *in situ* X-ray photoemission spectroscopy (XPS) and scanning tunneling microscopy (STM) measurements. Film orientation is characterized by *in situ* low-energy electron diffraction (LEED). In addition, Raman spectroscopy is used to identify vibrational mode of $PdTe_2$ thin film by comparing that of bulk $PdTe_2$. The band structure of few-layer $PdTe_2$ film is investigated by ARPES. We also show that these epitaxial $PdTe_2$ films have good air-stability and atomically clean surfaces can be easily restored by a mild annealing process after reloading the samples into ultrahigh vacuum (UHV)

*Project supported by the National Natural Science Foundation of China (Grant Nos. 61390501, 61622116, and 61471337), the Science Fund from the Chinese Academy of Sciences (CAS) (Grant Nos. XDPB0601 and XDPB0801), the CAS Pioneer Hundred Talents Program, and the Beijing Nova Program (Grant No. Z181100006218023).

†Corresponding author. E-mail: xlin@ucas.ac.cn
‡Corresponding author. E-mail: hjgao@iphy.ac.cn

chamber.

2. Method

Experiments were carried out in an Omicron UHV system equipped with STM and an MBE chamber for sample preparation. The base pressure of the system was better than 1.0×10^{-10} mbar (1 bar = 10^5 Pa). A nitrogen-doped 6H–SiC(0001) wafer (0.1 Ω·cm) was graphitized by flashing to 1550 K. This led to the formation of bilayer graphene (BLG),[24,25] which served as the substrate for $PdTe_2$ growth. BLG/SiC(0001) has been chosen as a substrate because it has the same crystal symmetry with (0001)-oriented $PdTe_2$ and can be easily achieved in UHV chamber, which makes it a widely used substrate for TMDs thin films growth.[5,10,26] The quality of bilayer graphene was checked by LEED and STM. High-purity Pd (99.95%, Alfa Aesar) and Te (99.999%, Sigma) sources were evaporated from electron-beam evaporator and standard Knudsen diffusion cell respectively, while the substrate was kept at 510 K during the growth process. Typical flux ratio between Te and Pd was $\sim 15:1$.

After growth, the sample was transferred to different chambers for LEED, STM, and ARPES characterizations. All STM measurements were performed at room temperature with a chemically etched W tip. The ARPES data were measured using an ultraviolet lamp with He Iα spectral line while the sample was maintained at 20 K. The energy analyzer was a VG Scienta R4000 with a total energy resolution set to be less than 20 meV. The XPS spectra were acquired at the Beijing Synchrotron Radiation Facility (BSRF). The samples were stored in a UHV suitcase during transfer among different experimental systems. The synchrotron radiation light monochromated by 4 high-resolution gratings and controlled by a hemispherical energy analyzer has a photon energy in a range from 10 eV to 1100 eV. The photon energies of XPS experiments were 500 eV for Pd 3d and 720 eV for Te 3d measurements, respectively. Raman spectra were acquired by a Renishaw spectrometer at 532 nm with about 1 mW power.

First-principles calculations were performed within the Vienna *ab initio* Simulation Package (VASP),[27] version 5.4.1, using the projector augmented-wave (PAW) method.[28] The plane-wave basis set with a kinetic energy cutoff of 400 eV. Electron exchange and correlation effects were treated using the generalized gradient approximation (GGA) functional of Perdew, Burke and Ernzerhof (PBE)[29] with spin-orbital coupling (SOC). The surface state was calculated by 6-layer $PdTe_2$ which was modeled by a periodic 1×1 slab geometry with a vacuum thickness of 18 Å. All the atoms were allowed to relax along the calculated forces of less than 0.01 eV/Å. A $15 \times 15 \times 1$ Gamma-centered k-point mesh was used to sample the Brillouin zone.

3. Results and discussion

As schematically illustrated in Fig. 1(a), bulk $PdTe_2$ crystallizes into the CdI_2 type (P_{3m1}) structure and consists of a hexagonally packed layer of Pd atoms sandwiched between two layers of Te anions, which is a typical 1T structure. Figures 1(b) and 1(c) show the typical STM topographic images of $PdTe_2$ films with different coverages. Initially, hexagonal islands, implying a hexagonal symmetry of $PdTe_2$ structure, are observed. At high coverage, continuous epitaxial layers form on graphene substrate as shown in Fig. 1(c). Figure 1(d) displays an atomically resolved STM topograph, showing a monoatomic step and revealing hexagonally arranged protrusions with a lattice constant of $\sim$ 4.0 Å. This value, together with a measured step height of 5.0 Å (the inset in Fig. 1(d)), matches well with those of (0001)-oriented bulk $PdTe_2$ (Fig. 1(a)).[30] Note that the bright spots in Fig. 1(d) correspond to the topmost Te atoms.

On the other hand, (0001)-oriented PdTe, a NiAs-type compound, has an in-plane lattice parameter close to that of $PdTe_2$ with a small difference of 0.1 Å,[30] which makes it difficult to distinguish it from STM results. To further confirm the chemical composition of our sample, we perform XPS measurements on both commercial bulk $PdTe_2$ and as-fabricated $PdTe_2$ films. Figures 1(e) and 1(f) show XPS spectra from the core level of the Pd 3d and Te 3d respectively, for bulk $PdTe_2$ (black curves) and epitaxial films (red curves). The curves of bulk and films show the accordance in characteristic peak positions and shapes for both Te and Pd. The Pd $3d_{5/2}$ core level in epitaxial film is detected at a binding energy of 336.9 eV, which is significantly different from the reported values (336.0 eV) for PdTe.[31] These combined STM and XPS results confirm the as-grown films to be $PdTe_2$ layers. Additionally, we find that experimentally it is easier to obtain the few-layer $PdTe_2$ films rather than the monolayer $PdTe_2$ films.

What is more, the structure of epitaxial $PdTe_2$ film is characterized by LEED. As shown in Fig. 2(a), the signals from the $PdTe_2$ film (indicated by yellow circles) and the graphene substrate (red circles) are observed. $PdTe_2$ grows mainly along the crystal orientation of the substrate with a tiny distribution of azimuthal angles because of the weak coupling between $PdTe_2$ and graphene, showing an arc-like feature in LEED spots. Epitaxial $PdTe_2$ has an incommensurate lattice with respect to graphene, similar to other layered TMDs films grown on graphene substrate.[32,33] These features, strain-free growth and no misfit dislocations despite large lattice mismatch, indicate that the growth of $PdTe_2$ film on graphene is a typical van der Waals epitaxy.[34] We also perform Raman measurements on as-fabricated $PdTe_2$ films and bulk $PdTe_2$. As shown in Fig. 2(b), two prominent vibrational modes are visible in as-fabricated films, at ~ 82.3 cm^{-1} and ~ 133.2 cm^{-1}, corresponding to the in-plane (E_g) and out-of plane (A_{1g}) motions of

Te atoms,[35,36] respectively. In bulk $PdTe_2$, E_g and A_{1g} modes are pinned at ~ 75.5 cm^{-1} and ~ 133.2 cm^{-1}, respectively. By comparing the Raman spectra, we notice that A_{1g} mode remains unchanged and the E_g mode shifts from 75.5 cm^{-1} to 82.3 cm^{-1}. Similar results were reported in other TMD material with 1T structure like $PtSe_2$, whose A_{1g} mode remains unchanged and E_g mode has a blue-shift with thickness decreasing from 5 nm to 0.5 nm.[37] This blue-shift may be attributed to long-range Coulombic interactions and possible stacking-induced changes of the intralayer bonding.[38]

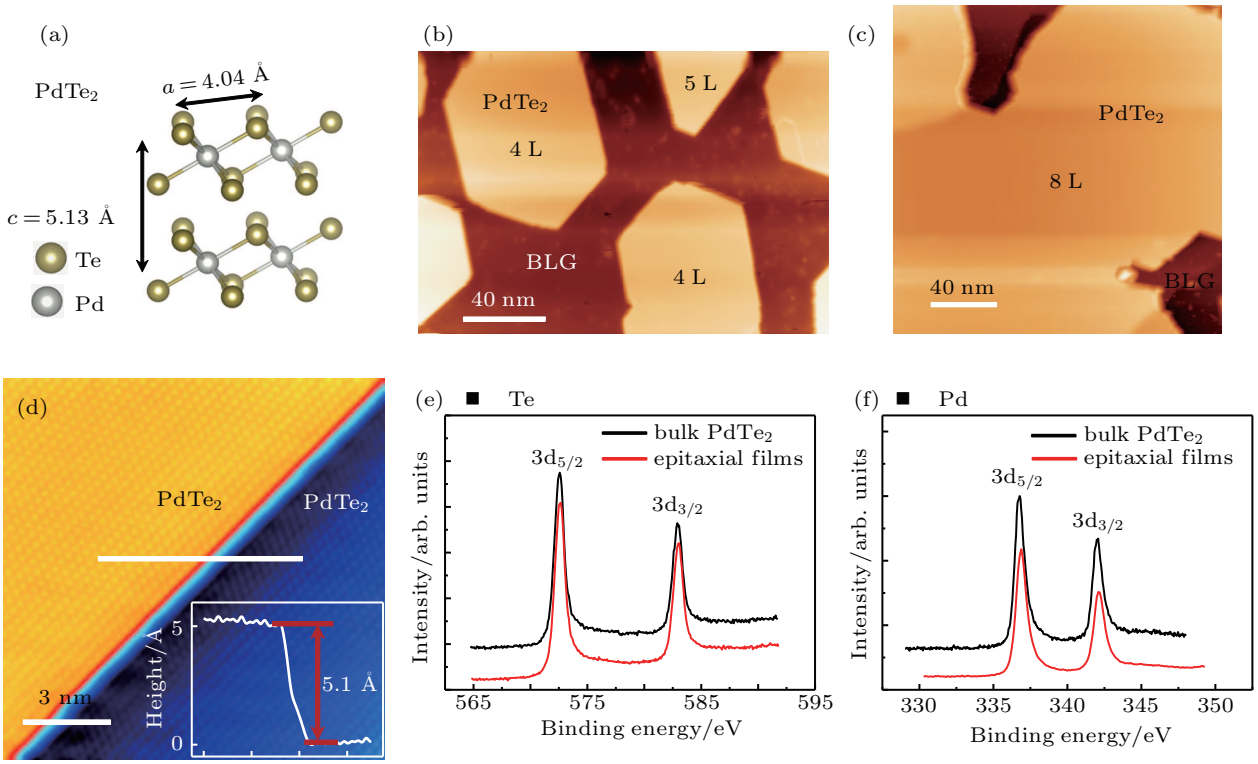

Fig. 1. (color online) Structures of $PdTe_2$ thin films grown on bilayer graphene (BLG). (a) Schematic crystal structure of $PdTe_2$ of side (bottom panel) view. [(b), (c)] STM topographic images (1.7 V, 80 pA) of epitaxial $PdTe_2$ films on bilayer graphene at (b) low coverage and (c) high coverage. Layer thickness is indicated in each panel. (d) Atomically resolved STM image (−780 mV, 1.6 nA) showing a terrace step. Inset displays line profile across the step. [(e), (f)] XPS results of bulk $PdTe_2$ (black curves) and epitaxial $PdTe_2$ films (red curves). (e) Te 3d core level spectra of bulk $PdTe_2$ and as-grown films. Characteristic peaks have the same positions at 572.5 eV ($3d_{5/2}$) and 582.9 eV ($3d_{3/2}$). (f) Pd 3d spectra of bulk $PdTe_2$ and as-grown films. Peak positions at 336.9 eV ($3d_{5/2}$) and 342.1 eV ($3d_{3/2}$) are also the same.

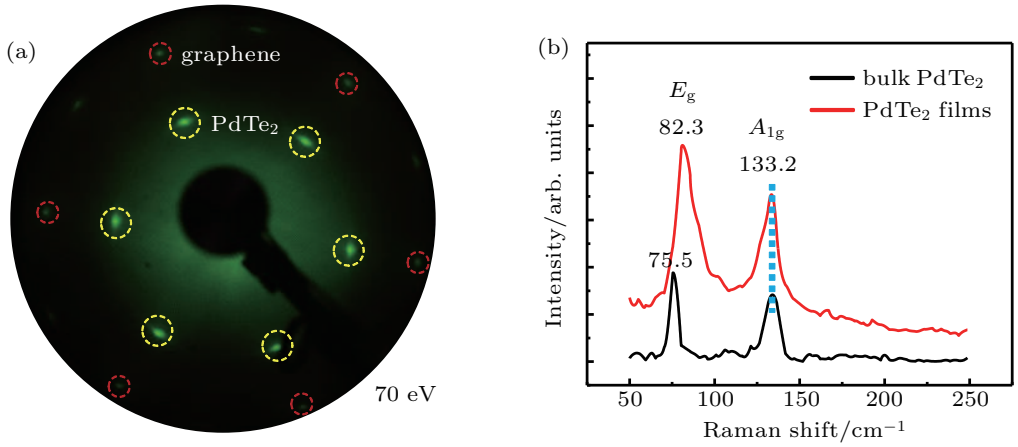

Fig. 2. (color online) Structure and vibrational modes of epitaxial $PdTe_2$ thin films. (a) LEED pattern of $PdTe_2$ film grown on bilayer graphene-SiC substrate. The red and yellow circles indicate the diffraction patterns of the graphene substrate and epitaxial $PdTe_2$ film, respectively. (b) Raman spectra of bulk and few-layer $PdTe_2$ films at room temperature.

Based on the STM, XPS, LEED, and Raman analysis, we conclude that we have grown high-quality few-layer $PdTe_2$ films by MBE. Then we investigate electronic energy band structure of $PdTe_2$ film with six layers by ARPES.

The electronic structure of bulk $PdTe_2$ has been investigated by ARPES measurement combing with first-principles calculations,[18,19,39] confirming a tilted type-II Dirac cone along the Γ–A direction and also a type-I Dirac cone with

Dirac point at ∼ 1.75 eV below Fermi level. Figure 3(a) shows the Fermi surface map acquired on a 6-layer $PdTe_2$ sample. The photoemission intensity map along the M–Γ–K direction is shown in Fig. 3(b). As the film thickness increases to 6 layers, additional quantum well states, or subbands, appear in the measured and calculated band structure as shown in Figs. 3(b) and 3(c). Furthermore, a conical dispersion at an energy between −1.5 eV and −2.5 eV is observed and denoted by red dashed lines in Fig. 3(b), which is a type-I Dirac cone with Dirac point located at about 1.75 eV below Fermi level. This originates from Z_2 topological surface state, which has been discussed in bulk $PdTe_2$ in detail.[39] The existence of the topological nontrivial surface state in a few-layer $PdTe_2$ film is also confirmed by the calculated surface state based on density functional theory (DFT) as shown in Fig. 3(c). Both the measured band structure and the calculated band structure reveal that the type I Dirac cone in 6-layer $PdTe_2$ has the same features as that in bulk $PdTe_2$.[39] A reduction in the film thickness (less than 5 layers) may lead to non-negligible overlapping between the surface-state wavefunctions from the two surfaces, which will give rise to a gap opening at the Dirac point.[40] Moreover, the existence of the substrate causes a potential difference between the two surfaces, which may lead to Rashba-type spin–orbit splitting.[40] Here we cannot check the possible changes because of the limitation to the number of obtained thinner $PdTe_2$ samples. As for the type-II Dirac cone, it is a tilted three-dimensional (3D) cone depending on $\boldsymbol{k}_z$ direction. When the bulk reduces to several nanometers, its band structure also becomes 2D, which means that there will no energy dispersion along $\boldsymbol{k}_z$ direction in atomic thin film. Therefore, we deduce that this type-II Dirac cone does not exist in few-layer $PdTe_2$ film.

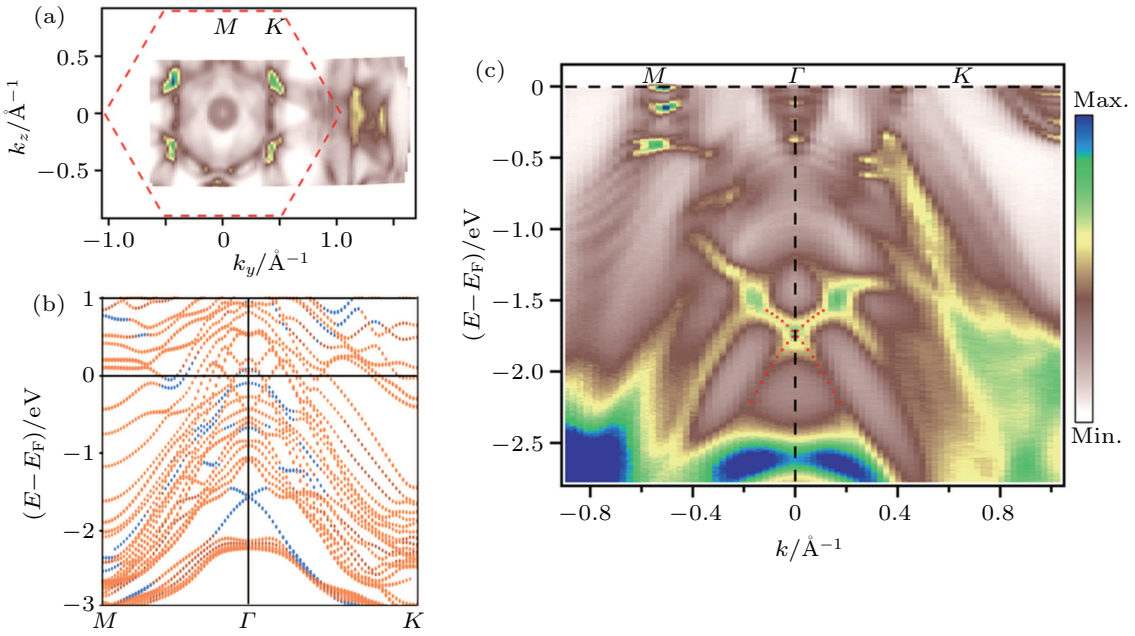

Fig. 3. (color online) ARPES maps and DFT calculations of the electronic structure of 6-layer $PdTe_2$ films. (a) Fermi surface map at photon energy of 21.2 eV. (b) Band structure measured along high symmetry directions. Red dashed lines on the top of photoemission image highlight the Dirac-cone surface state. (c) Calculated surface state of 6-layer $PdTe_2$ film by DFT calculations. Orange line refers to bulk state, while blue line represents surface state.

Moreover, air-stability is critical for 2D material in practical applications. Air-exposure experiments of the epitaxial $PdTe_2$ films are carried out. The samples are exposed to air and kept at room temperature for more than 5 h. After that, the sample is transferred back into the UHV chamber and mild annealing at 450 K is taken to remove possible physisorbed species. Figures 4(a) and 4(b) display large-scale and atomic-resolution STM images of $PdTe_2$ films after being annealed in UHV chamber. A clean and smooth surface can be identified. Meanwhile, LEED pattern also reveals a clean and sharp diffraction spot after being exposed to air. These combined STM and LEED measurements indicate the chemical robustness of the epitaxial $PdTe_2$ film.

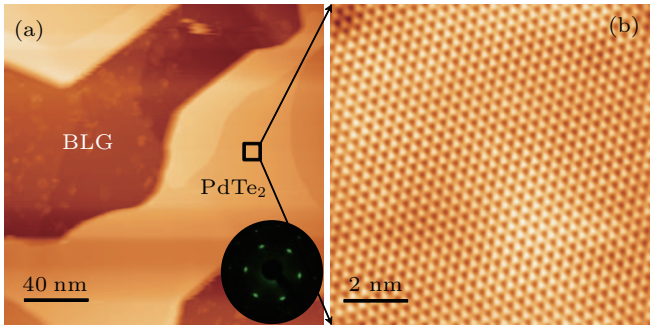

Fig. 4. (color online) Air stability of $PdTe_2$ thin film. (a) STM topographic image (−1.6 V, 0.1 nA) of sample after being exposed to air, showing clean and smooth surface. Inset shows a sharp and clean LEED pattern of $PdTe_2$ film on graphene substrate after being exposed to air. (b) Atomically resolved STM image (−787 mV, 1.6 nA) taken on a flat $PdTe_2$ terrace in panel (a).

4. Conclusions

In this work, $PdTe_2$ films on bilayer graphene-SiC(0001) substrates are fabricated by the MBE method. *In situ* LEED, STM, and XPS measurements demonstrate high quality of the epitaxial $PdTe_2$ films. Raman-active modes in $PdTe_2$, in-plane (E_g) and out-of plane (A_{1g}) motions, are analyzed and compared with those in bulk $PdTe_2$. ARPES measurement of a 6-layer $PdTe_2$ film reveals its metallicity and a type-I Dirac cone contributing from Z_2 topological surface state. Furthermore, air exposure experiments demonstrate the chemical stability of epitaxial $PdTe_2$ film. MBE growth of high quality $PdTe_2$ film make possible the *in situ* epitaxial antimonene growth in UHV chamber, building antimonene/$PdTe_2$ film heterostucture for applications in electronic and optoelectronic nanodevices.

Acknowledgment

This research was partly performed in CAS Key Laboratory of Vacuum Physics. Computational resources were provided by the National Supercomputing Center in Tianjin.

References

[1] Chhowalla M, Shin H S, Eda G, Li L J, Loh K P and Zhang H 2013 *Nat. Chem.* **5** 263
[2] Wang Q H, Kalantar-Zadeh K, Kis A, Coleman J N and Strano M S 2012 *Nat. Nanotechnol.* **7** 699
[3] Jariwala D, Davoyan A R, Wong J and Atwater H A 2017 *ACS Photon.* **4** 2962
[4] Mak K F, McGill K L, Park J and McEuen P L 2014 *Science* **344** 1489
[5] Ugeda M M, Bradley A J, Zhang Y, Onishi S, Chen Y, Ruan W, Ojeda-Aristizabal C, Ryu H, Edmonds M T and Tsai H Z 2016 *Nat. Phys.* **12** 92
[6] Sipos B, Kusmartseva A F, Akrap A, Berger H, Forro L and Tutis E 2008 *Nat. Mater.* **7** 960
[7] Chen P, Chan Y H, Fang X Y, Zhang Y, Chou M Y, Mo S K, Hussain Z, Fedorov A V and Chiang T C 2015 *Nat. Commun.* **6** 8943
[8] Ali M N, Xiong J, Flynn S, Tao J, Gibson Q D, Schoop L M, Liang T, Haldolaarachchige N, Hirschberger M and Ong N 2014 *Nature* **514** 205
[9] Wang Y, Li L, Yao W, Song S, Sun J, Pan J, Ren X, Li C, Okunishi E and Wang Y Q 2015 *Nano Lett.* **15** 4013
[10] Ugeda M M, Bradley A J, Shi S F, Felipe H, Zhang Y, Qiu D Y, Ruan W, Mo S K, Hussain Z and Shen Z X 2014 *Nat. Mater.* **13** 1091
[11] Zhang Y, Chang T R, Zhou B, Cui Y T, Yan H, Liu Z, Schmitt F, Lee J, Moore R and Chen Y 2013 *Nat. Nanotechnol.* **9** 111
[12] Roberts B W 1976 *J. Phys. Chem. Ref. Data* **5** 581
[13] Fei F, Bo X, Wang R, Wu B, Jiang J, Fu D, Gao M, Zheng H, Chen Y and Wang X 2017 *Phys. Rev. B* **96** 041201
[14] Frindt R 1972 *Phys. Rev. Lett.* **28** 299
[15] Huang H, Zhou S and Duan W 2016 *Phys. Rev. B* **94** 121117
[16] Yan M, Huang H, Zhang K, Wang E, Yao W, Deng K, Wan G, Zhang H, Arita M and Yang H 2017 *Nat. Commun.* **8** 257
[17] Zhang K, Yan M, Zhang H, Huang H, Arita M, Sun Z, Duan W, Wu Y and Zhou S 2017 *Phys. Rev. B* **96** 125102
[18] Noh H J, Jeong J, Cho E J, Kim K, Min B and Park B G 2017 *Phys. Rev. Lett.* **119** 016401
[19] Clark O J, Neat M J, Okawa K, Bawden L, Marković I, Mazzola F, Feng J, Sunko V, Riley J M and Meevasana W 2018 *Phys. Rev. Lett.* **120** 156401
[20] Zhang S, Yan Z, Li Y, Chen Z and Zeng H 2015 *Angew. Chem.* **127** 3155
[21] Wu X, Shao Y, Liu H, Feng Z, Wang Y L, Sun J T, Liu C, Wang J O, Liu Z L and Zhu S Y 2017 *Adv. Mater.* **29** 1605407
[22] Chen X, Yang Q, Meng R, Jiang J, Liang Q, Tan C and Sun X 2016 *J. Mater. Chem. C* **4** 5434
[23] Pizzi G, Gibertini M, Dib E, Marzari N, Iannaccone G and Fiori G 2016 *Nat. Commun.* **7** 12585
[24] Wang Q, Zhang W, Wang L, He K, Ma X and Xue Q 2013 *J. Phys.: Condens. Matter* **25** 095002
[25] Riedl C, Starke U, Bernhardt J, Franke M and Heinz K 2007 *Phys. Rev. B* **76** 245406
[26] Peng J P, Guan J Q, Zhang H M, Song C L, Wang L, He K, Xue Q K and Ma X C 2015 *Phys. Rev. B* **91** 121113
[27] Kresse G and Furthmüller J 1996 *Phys. Rev. B* **54** 11169
[28] Blöchl P E 1994 *Phys. Rev. B* **50** 17953
[29] Perdew J P, Burke K and Ernzerhof M 1996 *Phys. Rev. Lett.* **77** 3865
[30] Predel B *Pd–Te (Palladium–Tellurium): Datasheet from Landolt-Börnstein — Group IV Physical Chemistry*, Volume 5I: "Ni–Np–Pt–Zr" in SpringerMaterials (Berlin Heidelberg: Springer-Verlag)
[31] Elvy S, Williams P and Buckley A 1996 *Surf. Interface Anal.* **24** 641
[32] Yan M, Wang E, Zhou X, Zhang G, Zhang H, Zhang K, Yao W, Lu N, Yang S and Wu S 2017 *2D Materials* **4** 045015
[33] Zhang Y, Ugeda M M, Jin C, Shi S F, Bradley A J, Martín Recio A, Ryu H, Kim J, Tang S and Kim Y 2016 *Nano Lett.* **16** 2485
[34] Walsh L A and Hinkle C L 2017 *Appl. Mater. Today* **9** 504
[35] Kolobov A V and Tominaga J 2016 *Two-Dimensional Transition-Metal Dichalcogenides*, Vol. 239 (Springer)
[36] Vymazalová A, Zaccarini F and Bakker R J 2014 *Eur. J. Mineral.* **26** 711
[37] O'Brien M, McEvoy N, Motta C, Zheng J Y, Berner N C, Kotakoski J, Elibol K, Pennycook T J, Meyer J C and Yim C 2016 *2D Materials* **3** 021004
[38] Lee C, Yan H, Brus L E, Heinz T F, Hone J and Ryu S 2010 *ACS Nano* **4** 2695
[39] Liu Y, Zhao J Z, Yu L, Lin C T, Liang A J, Hu C, Ding Y, Xu Y, He S L, Zhou L, Liu G D, Dong X L, Zhang J, Chen C T, Xu Z Y, Wen H M, Dai X, Fang Z and Zhou X J 2015 *Chin. Phys. Lett.* **32** 067303
[40] Zhang Y, He K, Chang C Z, Song C L, Wang L L, Chen X, Jia J F, Fang Z, Dai X and Shan W Y 2010 *Nat. Phys.* **6** 584